PHYSICAL REVIEW B VOLUME 56, NUMBER 7 15 AUGUST 1997-I

Initial growth morphology in a heteroepitaxial system at low temperature: Fe on Ag(100)

M. Canepa, S. Terreni, P. Cantini, Andrea Campora, and L. Mattera
Istituto Nazionale di Fisica della Materia and Centro di Fisica delle Superfici e Basse Temperature (CNR), Dipartimento di Fisica, Università di Genova, 16146 Via Dodecaneso 33, Genova, Italy

(Received 14 February 1997)

The growth of ultrathin iron films on Ag(100) at 135 K has been studied by means of thermal-energy helium diffraction. Film deposition has been monitored by measuring the oscillations of the specular beam intensity during the growth. Information on the island morphology of the deposited film has been obtained by exploiting the dependence of the scattered intensity on the momentum transfer. The set of data indicates that there are definite differences between the growth mode of the first and subsequent layers. The surface of the first monolayer exhibits a two-dimensional morphology, while the estimate of the interface width w [J. W. Evans, Phys. Rev. B **43**, 3897 (1991)] from a kinematic analysis of data provides values of w^2 ranging from 0.28 at 2 ML to 0.37 at 5 ML. The obtained values are consistent with the so-called one-hop transient mobility model with adsorption at the fourfold hollow site and show that from the second layer on the morphology gradually deviates towards island growth. The analysis of rocking curves also provides the step height (h') of the growing interface. At 2, 3, 4, and 5 ML, h' assumes values that are slightly larger than the value of bulk bcc iron $h_{\mathrm{Fe}} = 1.43$ Å. This finding is assigned to the occurrence of intermixing through simple arguments based on the conservation of the atomic volumes. The Ag population at the surface of the film is found to decrease with film thickness consistently with recent ion-scattering measurements. [S0163-1829(97)04732-2]

I. INTRODUCTION

The epitaxial growth of ultrathin, magnetic metal films on nonmagnetic substrates has been attracting an exponentially increasing amount of research.[1] In this field, the connections between fundamental and applied studies are tight and an improvement of the knowledge on the growth process at the atomic level and on the interplay between morphologic and magnetic properties is expected to provide relevant inputs for applications in thin-film devices. The morphology of epitaxial films is affected by a variety of parameters. A list, surely incomplete, of such factors should include substrate quality, geometrical matching and chemical interaction between adsorbate and substrate, temperature and rate of deposition, film thickness, annealing procedures, and the promoting action of surfactants. The limited understanding of the complex correlations within such a large set of variables is invoked to account for the often controversial phenomenology that has been reported for many systems. In this respect, the attempt to correlate information deriving from complementary experimental tools obtained under comparable experimental conditions seems to be promising. We have followed this approach in our investigation of the growth of ultrathin Fe films on Ag(100).

Iron films on noble-metal surfaces occupy an outstanding rank in fundamental studies in the field of low-dimensional magnetism.[2] Moreover, they represent a fertile ground to face problems of primary interest in heteroepitaxy such as growth modes, structure of ultrathin films,[3] and processes such as interdiffusion and segregation that affect the sharpness of interfaces.

In our experiments structural properties are investigated by high surface sensitivity methods as thermal energy atom (He) scattering (TEAS) and low-energy ion scattering (LEIS). TEAS is employed to monitor the film growth during deposition and to study both the vertical roughness of the growing interface and the long-range order of the surface of films; LEIS allows the determination of elemental composition and surface structure.[4] Electronic states are investigated by a combined use of angle-resolved ultraviolet photoemission spectroscopy (ARUPS) and metastable deexcitation spectroscopy (MDS).[5] Finally, surface magnetism is investigated by spin-polarized MDS.[6]

In introductory papers[4,5] we showed that thermally driven Fe/Ag interdiffusion and Ag surface segregation are substantially ''frozen'' at temperatures lower than 200 K. Similarly to the Fe/Cu system,[7] the best strategy to grow a quality iron film on Ag(100) seems to consist of two main steps: deposition at low temperature, to minimize intermixing, followed by moderate annealing to improve the structural order avoiding, in the meantime, to trigger the segregation process.

This paper deals with a helium scattering study of the growth of ultrathin iron films deposited at 135 K on a well-characterized Ag(100) substrate. The complex effects produced by annealing on the morphology of films are currently under investigation and will be addressed elsewhere.

TEAS has been applied to a number of homoepitaxial systems while applications to heteroepitaxy are still relatively rare.[8] Our paper provides an example of a systematic application of *simple* kinematic theory concepts to helium scattering in the study of a complex heteroepitaxial system. Our results offer insight into intricate and open problems in the Fe/Ag growth morphology[9,10] and contribute to the open and interesting debate about the factors that improve the smoothing of the growing film and sustain the observation of diffraction intensity oscillations during growth at low substrate temperatures.[11]

The outline of the paper is as follows. In Sec. II some general aspects of diffraction from a stepped surface are briefly reviewed. Details on the experimental procedure together with a characterization of the substrate are given in Sec. III. Data are presented and discussed in Secs. IV and V, respectively. Finally, an outlook follows in Sec. VI.

II. DIFFRACTION FROM STEPPED SURFACES

Diffractive methods can be fruitfully employed either to monitor the growth during deposition or to investigate the ''postgrowth'' surface structure and the statistical distribution of terraces.[12] The monitoring of the intensity of an appropriate diffraction spot (''deposition curve'') represents a meaningful and direct method to control epitaxy.[13,14] Layer-by-layer (LBL) growth induces oscillations in the deposition curve that reflect the oscillations of the surface step density consequent to cyclical nucleation and coalescence of two-dimensional islands. Instead, in the case of three-dimensional growth the deposition curve decreases exponentially.

In view of the forthcoming presentation of the postgrowth analysis of films, we believe that it can be useful to review some basic theoretical aspects of diffraction from so-called randomly stepped surfaces. We initially consider chemically homogeneous surfaces, addressing, for a comprehensive treatment, a number of classical papers.[15,16] When the typical terrace size is much larger than the step edge region, it is possible to treat separately scattering from terraces and scattering from edges.[17] The former is concentrated in the vicinity of the Bragg directions pertinent to the defect-free surface, while edge scattering is angularly diffuse and causes an intensity attenuation of the Bragg spot.

The intensity profile measured across a diffracted spot consists of two contributions: a sharp central spike (a δ function in an ideal experiment) arising from the long-range surface order and a broad component that reflects the lateral step correlation. Provided that the form factor (the corrugation of the surface unit cell for atom-surface scattering) varies slowly with the momentum tranfer $\vec{S}=\vec{k}_f-\vec{k}_i$, the dependence of the specular intensity on $\vec{S}$ is mainly determined by the interference between waves scattered from different terrace levels and by the size distribution of terraces. The single-scattering approximation is the appropriate limit for large and flat terraces and is able to describe the variation of specular intensity as a function of $\vec{S}$ arising from surface topography (with the relevant exception of large angles of incidence of the beam where multiple-scattering effects can no longer be ignored). Hereafter we adopt the Lent-Cohen[16] approach as recently revisited in a helium diffraction experiment on the growth of iron on Cu.[18]

The specular intensity for a surface involving N *exposed* terrace levels, separated by steps of height h, can be written as[16]

$$I_0(\vec{S})=\left\{\delta(\vec{S}_{\parallel})\left[c_0+\sum_{l=1}^{N-1}2c_l\cos(S_z lh)\right]\right\}+\left\{\sum_{l=1}^{N-1}2c_lF_l(\vec{S}_{\parallel})[1-\cos(S_z lh)]\right\}, \tag{2.1}$$

where the first and second terms in curly brackets represent the central spike and the broad component, respectively. Both terms oscillate as a function of the perpendicular momentum transfer S_z. Oscillations are driven by the interference between waves scattered from terraces separated by multiples l of the step height h. When $S_z lh=2n\pi$ the interference is constructive (the *in-phase* condition); the peak shape is not affected by disorder and reduces to a δ function. If $S_z lh=2(n+1)\pi$ then the interference is destructive (the *antiphase* condition); the effect of the disorder is maximum so that diffraction becomes very sensitive to the presence of steps on the surface. At fixed S_z the intensity of the δ-like term depends only upon the coverage of the exposed terraces as[16]

$$c_l=\sum_{i=1}^{N-l}\theta_i\theta_{i+l}\quad(l=0,1,2,\dots), \tag{2.2}$$

where θ_i is the coverage of the ith exposed level.[19]

It is worth mentioning that in the case of ideal layer-by-layer growth, at most two levels, say, 1 and 2, are exposed at any time; when the two levels are equally populated (half integer coverages) and *antiphase* conditions are matched, the central spike vanishes completely. Therefore, *antiphase* conditions are the best circumstances in which to resolve oscillations in deposition curves.

The shape of the broad component reflects the statistical terrace distribution via the Fourier transform F_l of the correlation function between terraces separated by height lh. Therefore, the size distribution of terraces is reflected in spot profiles via the dependence of the specular intensity on $\vec{S}_{\parallel}$, the momentum transfer parallel to the surface. The vertical distribution of terraces instead is directly reflected in ''rocking curves'' via the dependence of the specular intensity on the perpendicular momentum transfer S_z. Before comparing measured intensities with Eq. (2.1) it is necessary to take into account the finite response of the detector and the effect of thermal vibrations. Concerning the former point, Eq. (2.1), after convolution with the response $A(\vec{S}_{\parallel})$ of the diffractometer, can be written as

$$I_0(\vec{S})=A(\vec{S}_{\parallel})\left[c_0+\sum_{l=1}^{N-1}2c_l\cos(S_z lh)\right]+\sum_{l=1}^{N-1}2c_lB_l(\vec{S}_{\parallel})[1-\cos(S_z lh)], \tag{2.3}$$

In Ref. 18 expression (2.3) is reformulated to obtain the intensity dependence on S_z at the specular position ($\vec{S}_{\parallel}=0$) as

$$I_0(S_z)=a_0+\sum_{l=1}^{N-1}a_l\cos(S_z lh), \tag{2.4}$$

where

$$a_0=Ac_0+\sum_{l=1}^{N-1}2c_lB_l \tag{2.5}$$

and

$$a_l=2c_l(A-B_l). \tag{2.6}$$

The coefficients a_l depend on the occupancy of terraces and on the step-step correlation.

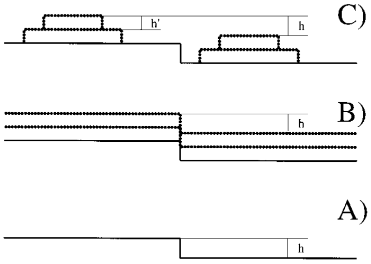

FIG. 1. Pictorial representation of the growth process. (a) The bare substrate with step height h is represented. (b) Ideal layer-by-layer (or 2D) growth: the deposit uniformly ''copies'' the substrate terrace structure. h is the step height relevant for interference effects in helium scattering. (c) Island (or 3D) growth. The deposit forms pyramids of typical step height h'. Both h and h' affect interference paths.

Thermal motion induces a monotonic variation of reflectivity as a function of S_z. At fixed temperature T the elastic specular intensity I_0^T can be written as[20]

$$I_0^T = I_0^0 \exp[-\alpha(T) S_z^2], \tag{2.7}$$

where I_0^0 represents the specular intensity that would be measured from a static surface. Finally, combining Eqs. (2.4) and (2.7) we obtain

$$I = I_0^T = a_0 \exp[-\alpha(T) S_z^2]\left[1+\sum_{l=1}^{N-1}\frac{a_l}{a_0}\cos(S_z l h)\right]. \tag{2.8}$$

Concerning heteroepitaxial growth, additional aspects should be dealt with. Let us begin by considering an ideally sharp interface. In the case of layer-by-layer growth, at the completion of each layer the film morphology ''copies'' the substrate layer [Figs. 1(a) and 1(b)]. In realistic cases, even in the presence of a good matching of in-plane lattice constants, the substrate and the growing film may be characterized by different interlayer distances. If the average dimension of substrate terraces is much larger than the transfer width[21] of the diffractometer, interference arises only from terraces of the growing film. If the average dimension of substrate terraces instead is comparable to the transfer width, it is in principle possible to observe a coupling between interference related to the substrate terrace structure and to the growing film steps [Fig. 1(c)]. Moreover, the step height, at least for ultrathin films, might significantly vary with film thickness, resulting in intricate interference patterns.

In the case of inhomogeneous surfaces, information on the spatial distribution of different scatterers can, in principle, be derived from spot profiles. Wollschläger *et al.*[22] showed in fact that the electron diffraction peak from an inhomogeneous stepped surface consists of the Bragg δ-like peak and two broad components related to steps and inhomogeneities distributions, respectively. While the component related to steps vanishes at in-phase conditions, the one due to inhomogeneities is independent of phase. Therefore, in favorable cases, step-induced and inhomogeneity-induced contributions can be effectively decoupled.[22,23]

Finally, we would like to mention that a criterion that can be effectively used to judge the dimensionality of the growth process, either in homoepitaxial or heteroepitaxial growth, is based on the evaluation of the surface roughness as a function of coverage. The interface roughness is quantified through the so-called interface width w, defined as the root-mean-square variation of the vertical width of the growing interface[19]

$$w^2 = \sum_{j=0}^{\infty} (j-\overline{J})^2 \theta_j, \tag{2.9}$$

where $\overline{J}=\sum_{j=1}^{\infty} j\theta_j$ is the total coverage. w^2 is a cyclical function of coverage with periodicity of 1 ML in the case of LBL growth, while it increases monotonically for three-dimensional growth.[19]

III. EXPERIMENT

Details on the experimental setup can be found elsewhere;[24] here we briefly review the main information relevant to the present experiment. The base vacuum in the analysis chamber is less than 10^{-10} Torr. The crystal is mounted on a manipulator that enables three rotations and a ± 5-mm translation along the direction normal to the sample. The temperature of the sample can be varied between 120 K and 1000 K. A nozzle-skimmer source provides a supersonic helium beam ($E_{\mathrm{He}} = 17.8$ meV, $\Delta v/v = 1\%$ full width at half maximum when the beam source is in thermal contact with a cryostat filled with liquid nitrogen). The in-plane angular distributions of scattered He atoms are detected by a rotatable, differentially pumped, quadrupole mass spectrometer with an acceptance angle of 2×10^{-4} sr. The transfer width of the He diffractometer, evaluated on the specular peak at 65° of incidence with $E_{\mathrm{He}} = 17.8$ meV, is of the order of 250 Å.

The single-crystal Ag(100) surface has been preliminarly prepared by prolonged sputtering and annealing cycles in a preparation chamber. The last stages of preparation in the analysis chamber have been accurately monitored by He scattering, LEIS,[4] and ARUPS.[5] The convergence of the preparation process is judged by maximizing the intensity and by minimizing the angular width of the reflected helium beam. At convergence, a peak profile analysis[21] gives an average width of terraces of the order of 350 Å, in good agreement with what is expected from the known miscut angle of the sample ($\pm 0.5°$). The Ag(100) surface behaves as a quasiperfect mirror for He. The intensity of diffraction peaks is typically a few thousandths of the specular beam intensity.

Additional useful information on the morphology of the substrate was obtained by the analysis of the specular TEAS rocking curve. Results are reported in Sec. IV. Films were grown at $T_{dep} = 135$ K. Coverage calibration, obtained by looking at TEAS ''deposition curves,'' is also reported in Sec. IV.

The Fe source, of the electron bombardment type, provides fluxes in the range 0.1–10 ML/min. In the present experiment typical fluxes of 0.5–1 ML/min were adopted with a dissipated power of the order of 20–25 W. After thoroughly outgassing the source, the pressure in the main chamber remains well below 5×10^{-10} Torr within 20 min of operation.

The cleanliness and stability of films have been monitored

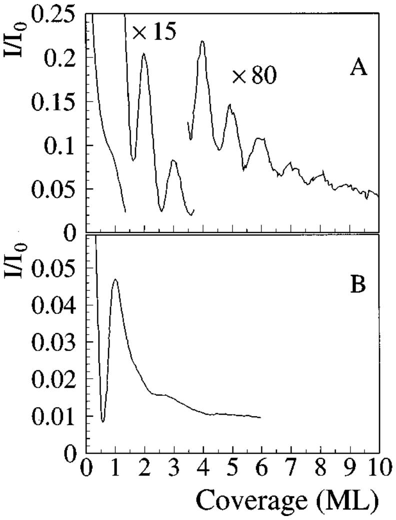

FIG. 2. Representative helium scattering deposition curves (intensity of the specular beam vs coverage). (a) Curve taken for $\gamma_i = 63°$ ($k_i = 5.85$ Å^{-1}). Up to nine damped oscillations are appreciable, though the first one is not resolved. (b) Curve taken for $\gamma_i = 50°$ ($k_i = 5.85$ Å^{-1}). In this kinematic condition the first oscillation is clearly visible, while subsequent oscillations are not resolved.

by ARUPS, MDS, LEIS, and TEAS. As iron films are very reactive towards background species, we have limited the measurement time after evaporation to 30–40 min in order to minimize contamination. Substrate conditions are restored by sputtering and annealing cycles. LEIS provides a careful elemental check capable of revealing residual surface Fe concentrations of the order of 0.1%. Efficient criteria are also provided by ARUPS.[5] Finally, the intensity and width of the helium specular peak provide a severe check on the retrieval of the long-range order of the substrate.

IV. RESULTS

A. Deposition

As anticipated in Sec. II, the best way to observe oscillations of the deposition curve is to choose antiphase kinematic conditions.[25] In this experiment, however, an extensive check performed by varying the angle of incidence γ_i (and therefore the S_z value) of the He beam has shown that antiphase conditions depend on the film thickness.

In Fig. 2(a) we show the deposition curve taken at $\gamma_i = 63°$. This angle turned out as the ''optimum'' condition to observe oscillations in deposition curves. Up to nine damped oscillations are observed, but the first one is not resolved. On the contrary, the first oscillation is clearly visible in Fig. 2(b) ($\gamma_i = 50°$), while the oscillation after the first one is badly resolved.

A better ''initial'' order of the substrate, evaluated by the intensity and the width of the specular peak prior to any exposure, leads to more intense oscillations. The intensity is generally reduced by the controlled addition of low levels of contaminants in the background gas during deposition. However, even in the best conditions, helium reflectivity is severely attenuated during growth. This indicates a growing average density of surface defects. At the same time, the presence of well-defined oscillations indicates a propensity to two-dimensional (2D) growth that becomes more and more feeble with exposure. The observation of regularly spaced oscillations, though damped, allows the coverage calibration. We assigned the coverage of 1 ML equivalent to the first maximum in Fig. 2(b). After this choice, the 2–9 ML correspond to the maxima of Fig. 2(a).

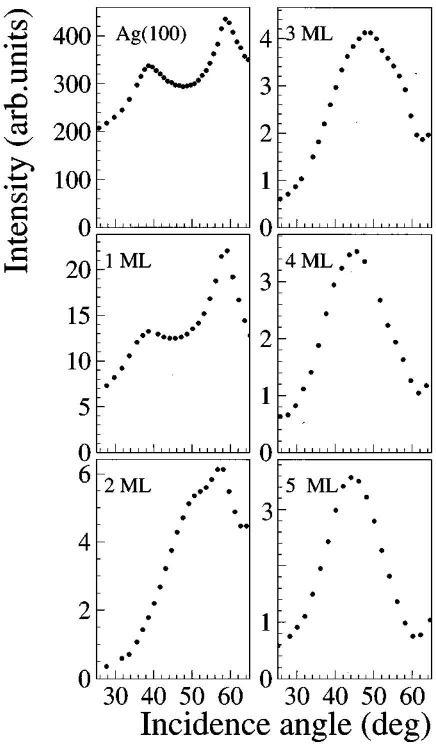

FIG. 3. Specular beam intensity as a function of the incidence angle γ_i (rocking curves) measured at 135 K on films of increasing thickness. The dependence of the intensity on the perpendicular component of the exchanged momentum (S_z) can be exploited through the relation $S_z = 2k_i \cos\gamma_i$.

B. Postgrowth He diffraction data

Figure 3 shows the rocking curves measured at 135 K for several film thicknesses. The dependence of the intensity on S_z is detected by scanning the polar angle of incidence γ_i at fixed $k_i = 5.85$ Å^{-1} ($S_z = 2k_i \cos\gamma_i$).

Before coming to a quantitative analysis of the curves, let us comment on the overall figure. The rocking curve of the substrate shows two well-defined maxima that satisfy the constructive interference condition $S_z h = 2n\pi$ with $n = 2$ ($\gamma_i \simeq 58°$) and $n = 3$ ($\gamma_i \simeq 38°$), indicating $h \simeq 2.05$ Å, in good agreement with the Ag/Ag step height h_{Ag}. We can consider the above-mentioned maxima as markers of Ag/Ag steps. At 1 ML the period $S_z h$ of the oscillation in the rocking curve reproduces the period of the bare substrate. The similarity of the rocking curve obtained at 1 ML to the one observed at 0 ML is *per se* a remarkable finding; in fact, it necessarily means that the first layer copies rather well the terrace morphology of the substrate, indicating a propensity to 2D growth. As the thickness increases from 1 to 5 ML the data show evident changes. The maxima typical of Ag/Ag steps decrease with coverage. Instead a ''new'' maximum

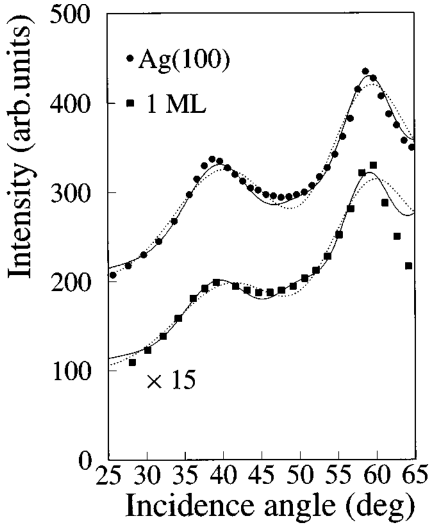

FIG. 4. Comparison between the experimental and the calculated rocking curves for the bare substrate (full circles) and the first monolayer film (full squares). Continuous lines represent Eq. (2.8) with $N=3$ and a_0, α, b_1, b_2, h taken as free parameters to fit the experimental rocking curves. Dotted lines represent Eq. (2.8) with $N=2$ (see the text).

progressively sets up at $\gamma_i \approx 45°$ from 2 ML on. These features clearly suggest that, in the range between 2 and 5 ML, interference paths arising from levels with different step height occur.

1. The substrate and the first ML

The rocking curve measured on the bare substrate (0 ML) was fitted by Eq. (2.8) with $N=3$, $b_1=a_1/a_0$, and $b_2=a_2/a_0$,

$$I=a_0\exp(-\alpha S_z^2)[1+b_1\cos(S_z h)+b_2\cos(2S_z h)], \tag{4.1}$$

an expression that is suitable for a system with three levels of terraces and steps of height h. a_0, α, b_1, b_2, and h were taken as free parameters. Minimization of χ^2 has been achieved by the routine MINUIT.[26] The best fit curve is shown in Fig. 4 as a continuous line. Information on the surface morphology is given by the parameters h, b_1, and b_2, which determine the period and the amplitude of the oscillations of the rocking curve; their fit values can be found in Table I. The factor $a_0\exp(-\alpha S_z^2)$ introduces only a smooth dependence on S_z without affecting the other parameters.

The addition of further terms in the cosine series does not improve the quality of the fit. On the contrary, the main features of the data are reproduced also by a simple two-level description (setting $b_2=0$). The best fit curve obtained in this case is shown in Fig. 4 (dotted line) for $b_1=0.136$ and $h=2.053$ Å. In both cases the values found for h are in good agreement with h_{Ag}.

TABLE I. Values of coefficients of Eq. (4.1) obtained by fitting the experimental rocking curves taken on the bare Ag(100) surface and after deposition of the first ML.

$\bar{J}$ (ML)	b_1	b_2	h (Å)
0	0.13±0.01	0.03±0.01	2.05±0.05
1	0.14±0.01	0.05±0.01	2.04±0.05

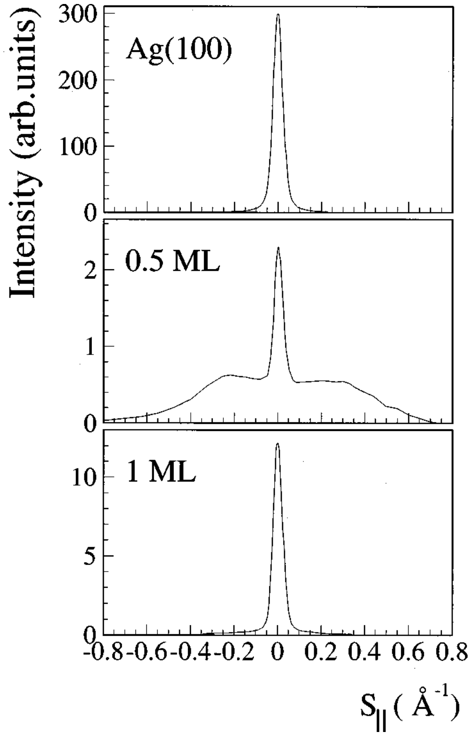

FIG. 5. Specular beam spot profiles taken, under *antiphase* conditions, at 0 ML ($\gamma_i=47°$), 0.5 ML ($\gamma_i=50°$), and 1 ML ($\gamma_i=47°$). The satellite structures at the sides of the Bragg spike at 0.5 ML indicate the presence of small islands. An estimate based on the angular positions of these satellites gives a size distribution peaked around a dimension of 15–20 Å.

The similarity of the rocking curve obtained at 1 ML to the one observed at 0 ML suggested the fit of the 1 ML rocking curve with the same equation assumed for the substrate. The best fit curve obtained for $N=3$ is shown in Fig. 4 as a continuous line. As shown in Table I, the parameters related to surface morphology assume values very close to those obtained at 0 ML, in spite of the strong reduction of intensity.

Again, the main features of the data are reproduced also by a simple two-level description ($N=2$). The best fit curve obtained in this case for $b_1=0.145$ and $h=2.050$ Å is shown in Fig. 4 as a dotted line.

Further support of the 2D-like growth of the film up to 1 ML comes from the analysis of specular spot profiles. In Fig. 5 we report the specular spot profiles taken, under antiphase conditions, at 0, 0.5, and 1 ML. At 0.5 ML we find an evident broad component and a δ peak of very low intensity (it should vanish for an ideal 2D growth and 0.5 coverage). The satellite structures at the sides of the Bragg spike indicate the presence of small islands.[27] An estimation based on the angular positions of these satellites gives a size distribution peaked around a dimension of 15–20 Å.[28]

The ''δ-like'' profile at 1 ML is very similar to the one taken on the bare substrate. This indicates that the surface is not rough despite the strong attenuation of the specular intensity. Nevertheless, this attenuation indicates that the 1-ML film exhibits defects that displace intensity from the Bragg peak to the diffuse background. We will return to this point in Sec. V.

2. The second and subsequent monolayers

As expected from an inspection of Fig. 3, the functional form adopted at 0 and 1 ML is not suitable for the rocking curves taken at 2, 3, 4, and 5 ML. Starting from the second monolayer, the film does not fit exactly the substrate morphology anymore and a new step height (h') appears. This means that occupancy of the $(N+1)$th level starts before the completion of the Nth one. The growth progressively loses the 2D character and the interface width increases with coverage.

Data analysis using formula (2.8) is still possible once a generalization to take into account the contemporary observation of step heights h and h' is introduced. In principle, we should consider the expression

$$\begin{aligned} I = a_0 \exp(-\alpha S_z^2)[1 + a\cos(S_z h) + b\cos(2S_z h) + c\cos(S_z h') \\ + d\cos(2S_z h') + e\cos[S_z(h+h')] + f\cos[S_z(h-h')] \\ + g\cos[S_z(h+2h')] + \cdots] \end{aligned} \tag{4.2}$$

appropriate for a three-level system with step height h' grown upon the terraces of the substrate of step h. This expression is rather unmanageable. The simplest expression that reproduces, to a good degree of accuracy, the main characteristics of the whole set of data turns out to be

$$\begin{aligned} I = a_0 \exp(-\alpha S_z^2)[1 + b_1\cos(S_z h) + b_1'\cos(S_z h') \\ + b_2'\cos(2S_z h')], \end{aligned} \tag{4.3}$$

with $b_1 = a_1/a_0$, $b_1' = a_1'/a_0$, and $b_2' = a_2'/a_0$.

In Eq. (4.3) we have assumed that the interference related to the step h' is ''local'' between paths involving islands that rest on a single terrace of the substrate. In this way the interference due to the terrace profile of the substrate with the interference due to the growing film terraces is decoupled. Further, as the growing density of defects reduces the step correlation length, we have assumed that interference paths involving next-nearest-neighbor terraces (height difference $2h$) are suppressed. The addition of the $\cos[S_z(h+h')]$ and $\cos[S_z(h-h')]$ components leads to only a slight improvement of the fits at large values of S_z.

A comparison between data and calculations is shown in Fig. 6. The values of the parameters related to the surface morphology are reported in Table II, where the indicated errors account for experimental errors and fit uncertainty.

Consistently with the qualitative observations made above, we observe that the coefficients b_1' and b_2' increase with coverage, indicating an increasing roughness of the surface morphology. The values of h at 2 and 3 ML are compatible, within experimental and fit uncertainties, with the Ag/Ag step height h_{Ag}. We note, however, a ''systematic'' lowering of this parameter with thickness. A systematic trend is observed also for h', which passes from 1.62 ± 0.05 Å at 2 ML to 1.53 ± 0.05 Å at 5 ML. The values of h' are somewhat larger than the bulk interlayer spacing of bcc Fe (1.43 Å). This finding seems to indicate a slight variation of h' with coverage.

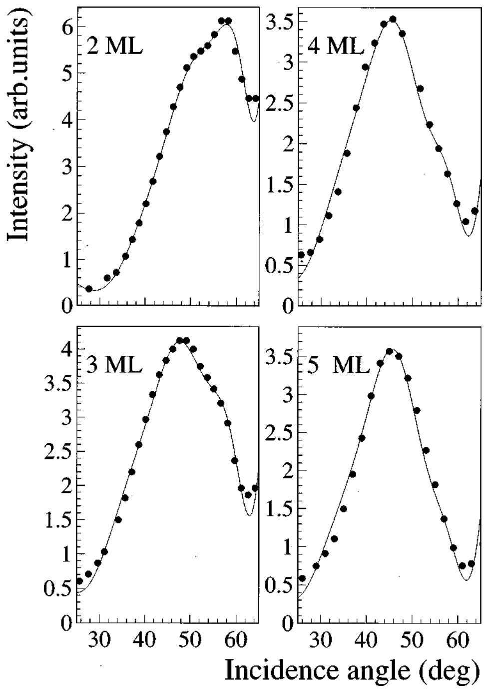

FIG. 6. Comparison between the experimental (full circles) and the calculated (lines) rocking curves for 2, 3, 4, and 5 ML. Equation (4.3) was fitted (lines) to the experimental rocking curves. The values of the parameters pertinent to the surface morphology can be found in Table II.

V. DISCUSSION

One of the main points that emerges from the data presented is that the first ML covers the substrate without modifying the terrace morphology, as expected in the case of 2D growth. In apparent contrast to what is expected for a 2D process, the specular intensity is drastically reduced (by a factor ≈ 20) during deposition of the first layer. The attenuation of the Bragg intensity could be due to defects that do not practically affect the interface width. Point defects (adatoms and/or vacancies) could be invoked to explain part of the attenuation of reflectivity[29] as well as the shape of islands.

At low temperature of growth, nucleated islands often display a rather irregular shape and even fractal or dendritic shapes have been detected in several homoepitaxial and heteroepitaxial systems.[30,31] We are unaware of the actual shape of islands in the present case, but we know that, at low temperature, the mean size of nucleated islands at 0.5 ML is very small (20 Å). We speculate that the shape of the coalescing islands is irregular and that at ''saturation'' of the first layer, residual ''fjords'' between islands could cause the attenuation of reflectivity without contributing to the terrace scattering.

Another factor that could explain the low helium reflectivity of the film is the inhomogeneity of the surface composition consequent to Fe/Ag exchange processes, already active during growth at temperatures as low as 135 K.[4,32] Even

TABLE II. Values of coefficients of Eq. (4.3) obtained by fitting the experimental rocking curves taken on films of increasing thickness.

$\overline{J}$ (ML)	b_1	b_1'	b_2'	h (Å)	h' (Å)
2	0.46±0.02	0.71±0.02	0.06±0.01	2.05±0.05	1.62±0.05
3	0.47±0.02	0.79±0.02	0.08±0.01	1.97±0.05	1.56±0.05
4	0.46±0.02	0.87±0.02	0.10±0.01	1.95±0.05	1.54±0.05
5	0.44±0.02	0.98±0.02	0.11±0.01	1.94±0.05	1.53±0.05

this kind of defect does not substantially affect the interface width.

The damping of deposition curves observed from 2 ML on suggests the so-called $2D_l$ regime,[33] experimentally characterized on homoepitaxial systems and extensively studied theoretically.[11,34,35] The number of resolved oscillations and the strength of damping qualitatively measure the quality of the layer-by-layer growth. At moderately low temperature (250–300 K), the damping is generally soft,[33,36,37] while it is stronger at temperatures in the 100–200 K range.[36,37]

Looking at the data of Sec. IV we note two facts. First, a single damping coefficient does not seem sufficient to describe both the strong decay of the reflectivity between 0 and 1 ML and the softer damping at larger coverages. Second, while the film surface appears smooth at 1 ML, the rocking curves at 2, 3, 4, and 5 ML provide neat indications of an increased surface roughness. We believe that while the strong decay of the intensity observed after deposition of the first monolayer is mainly due to defects that do not affect roughness, the softer damping between 2 and 5 ML could be ascribed, at least partially, to the increase of the interface width.

Concerning the interface width, we try a quantitative comparison of our experimental findings with calculations presented in a paper on metal-on-metal epitaxy on fcc(100) surfaces at low temperature.[11] In that paper Evans reviewed processes such as ''downward funneling''[19] and ''transient mobility,''[38] which mediate interface smoothness and favor quasi layer-by-layer growth at temperatures where thermal diffusion is negligible. Evans simulated several growth processes and calculated the interface width and the kinematic Bragg intensity as a function of coverage.

Due to the high sensitivity of He reflectivity to defects, including step edges, a direct comparison of experimental helium deposition curves and kinematic Bragg intensity calculations does not allow one to extract *quantitative* information on the interface roughness. We proceed instead to derive the interface roughness w from a quantitative analysis of the rocking curves.

We showed in Sec. IV B 2 that when the total coverage $\overline{J}$ equals 2, 3, 4, and 5 ML a three-level system rests on the substrate. If we disregard the roughness of the substrate and $\theta_{\overline{J}-1}$, $\theta_{\overline{J}}$, and $\theta_{\overline{J}+1}$ are the coverages of the three exposed levels, then $\theta_{\overline{J}-1}+\theta_{\overline{J}}+\theta_{\overline{J}+1}=1$ (see the Appendix). The interface width reads [see Eq. (2.9)]

$$w^2(\overline{J})=\theta_{\overline{J}-1}+\theta_{\overline{J}+1}. \tag{5.1}$$

At 2, 3, 4, and 5 ML the intensity of the broad component of the spot profiles has been found to be at most a few percent of the Bragg intensity. Therefore, as a first approximation, we can ignore B_l with respect to A in Eqs. (2.5) and (2.6). Within this approximation the rocking curve (4.3) reduces to

$$I\simeq Ac_0\exp(-\alpha S_z^2)\left[1+\frac{2c_1}{c_0}\cos(S_zh)+\frac{2c_1'}{c_0}\cos(S_zh')\right.$$
$$\left.+\frac{2c_2'}{c_0}\cos(2S_zh')\right], \tag{5.2}$$

where the experimentally determined coefficients of the cosine series depend on the levels coverage only [via Eq. (2.2)].

This allows us to obtain the values of $\theta_{\overline{J}-1}$, $\theta_{\overline{J}}$, and $\theta_{\overline{J}+1}$ that satisfy the set of equations (see the Appendix)

$$1=\theta_{\overline{J}-1}+\theta_{\overline{J}}+\theta_{\overline{J}+1} \tag{5.3}$$

$$b_1'=\frac{2c_1'}{c_0}=2\frac{\theta_{\overline{J}-1}\theta_{\overline{J}}+\theta_{\overline{J}}\theta_{\overline{J}+1}}{\theta_{\overline{J}-1}^2+\theta_{\overline{J}}^2+\theta_{\overline{J}+1}^2}, \tag{5.4}$$

$$b_2'=\frac{2c_2'}{c_0}=2\frac{\theta_{\overline{J}-1}\theta_{\overline{J}+1}}{\theta_{\overline{J}-1}^2+\theta_{\overline{J}}^2+\theta_{\overline{J}+1}^2}. \tag{5.5}$$

The condition $\theta_{\overline{J}}\geqslant\theta_{\overline{J}-1}+\theta_{\overline{J}+1}$ leads to a unique set of solutions. The values of $\theta_{\overline{J}}$ obtained are shown in Table III for $\overline{J}=2$, 3, 4, and 5 ML, together with the corresponding values of the interface width.

As a first comment to Table III we remark that $\theta_{\overline{J}}$, though slowly decreasing from 2 to 5 ML, remains substantially larger than $\theta_{\overline{J}-1}+\theta_{\overline{J}+1}$. This indicates that even at the fifth oscillation of the deposition curve, the system is still far from a 3D-like growth.

The calculated interface width w^2 slowly increases from 0.28 at 2 ML to 0.37 at 5 ML. The values of w^2 lie very close to the curve presented in Ref. 11 for the so-called one-hop transient mobility model with adsorption occurring on the fourfold hollow site, while they differ by approximately

TABLE III. Calculated interface width ($w^2=\theta_{\overline{J}-1}+\theta_{\overline{J}+1}$).

$\overline{J}$ (ML)	w^2	$\theta_{\overline{J}}$
2	0.28±0.01	0.72±0.01
3	0.30±0.01	0.70±0.01
4	0.33±0.01	0.67±0.01
5	0.37±0.01	0.63±0.01

-0.05 and $+0.05$ from the curves calculated for the downward funneling and the two-hop transient mobility models, respectively.

Rocking curves give the step height (h') of the growing interface with the relevant exception of the first ML as there the 2D growth provides only the step height h of the substrate. Information on this point has been extracted by a careful analysis of rocking curves at submonolayer coverages giving $h' = 1.76$ Å.[40]

Table II shows that the values of h' are slightly larger than the value $h_{\mathrm{Fe}} = 1.43$ Å of bulk bcc iron. In this respect, we consider a naive model based on the conservation of the atomic volumes. Jonker and Prinz[39] pointed out that, upon rotation of the α-Fe(100) plane by 45° with respect to the Ag(100) plane, the horizontal lattice mismatch is only 0.8%. According to these symmetry considerations, the fourfold hollow is the privileged adsorption site in the growth process. Considering the chance of Fe-Ag exchange at deposition we assume that, disregarding the small horizontal misfits, all Fe/Ag, Fe/Fe, and Ag/Fe structures are characterized by the same square cell. Under this assumption, intermixing is expected to affect only the vertical lattice spacings of the growing structure. The measured step heights are then considered as weighted averages of the bulk intralayer spacing of fcc Ag and bcc Fe (2.04 and 1.43 Å, respectively). The weights reflect the Fe and Ag concentrations inside the growing film. This simple model leads to Ag percentages ranging from ~55% at 1 ML, through 30% at 2 ML, up to 20% at 5 ML. The obtained values are in good agreement with the results provided by an ion scattering spectroscopy study of films (0–10 ML) grown under the same experimental conditions as the present ones,[4] which clearly demonstrate the occurrence of Fe-Ag intermixing.

One mechanism that is able to explain the intermixing at 135 K is a ''place exchange'' between the incoming Fe atom and a Ag atom on the surface.[32] Diffusion mediated by atomic place exchange (''exchange diffusion'') has been reported on a variety of homoepitaxial[41,42] and heteroepitaxial systems, even at low temperatures.[43,44] Further, ''exchange diffusion'' recently has been claimed for room-temperature growth of Fe on Au(001),[45] Ag(100),[46] and Cu(100).[47]

Finally, we comment on two other aspects that seem to be complementary to this work. The first one concerns the characterization of the growth mode at higher substrate temperatures. If the growth temperature is raised over $T \simeq 270$ K the deposition curves exhibit a rapid monotonic decay without any superimposed oscillation. An exponential decay is usually interpreted in terms of 3D island nucleation. We observe that the kind of analysis presented here becomes less and less adequate as the growth system moves far away from two dimensions. The 3D regime is probably driven by the increase of the typical size of nucleated islands.[28] This behavior is common to other systems, for example, Pt/Pt(111).[33] However, in contrast to other systems, deposition curve oscillations do not reappear at higher growth temperatures. Intense Fe/Ag interdiffusion demonstrated by ARUPS data[5] is expected to be a key process involved in the absence of a 2D regime at high temperature.

The second point concerns the effects of annealing. There is an obvious interest about the role of thermal diffusion in the modifications of morphology and composition of the films deposited at low temperatures. Measurements on this point are in progress. Preliminary results, obtained by the combined application of helium scattering, ion scattering, and photoemission spectroscopies suggest an interplay between morphologic ordering and intermixing. In particular, annealing at room temperature, even prolonged, seems insufficient to ensure a long-range surface ordering of films; though the specular peak intensity increases from the low-temperatures values, it still remains very low (two orders of magnitude with respect to the Ag substrate at the same temperature), indicating a rather faulty surface. Surface ordering requires higher annealing temperatures (typically 500 K), but it is accompanied by intense Fe/Ag mixing with Ag segregation at the surface. A satisfactory model of this aspect requires further experimental investigation and interpretative effort.

VI. SUMMARY AND CONCLUSIONS

We have presented a helium scattering study on the growth of ultrathin iron films on Ag(100) at 135 K. Film deposition is monitored in real time by measuring the oscillations of helium reflectivity. The morphology of the deposited film is investigated by exploiting the dependence of the scattered intensity on the momentum transfer.

The experimental data reflect definite differences between the growth mode of the first and subsequent layers. At 1 ML, in spite of a strong decay of the specular intensity with respect to the bare substrate, we have found a 2D morphology. Early stages of growth are characterized by nucleation of many small 2D islands (typical dimension are approximately equal to 20 Å at 0.5 ML). The small island size, especially if coupled to an irregular shape, could explain 2D growth through transient mobility. Between 2 and 5 ML where morphology gradually deviates from the 2D growth towards island growth, the damping of the specular intensity is reduced and seems to be explained by the slow increase of the interface width.

We presented an estimate of the interface width from the analysis of rocking curves taken on completed layers. The values obtained, ranging from 0.28 at 2 ML to 0.37 at 5 ML, are consistent with the so-called one-hop transient mobility model with adsorption at the fourfold hollow site.

The results therefore rule out Frank–Van Der Merwe and Volmer-Weber growth processes whereas they seem to resemble the Stranski-Krastanov growth mode with a 2D growth of the first layer followed by some degree of 3D island formation. However, consistently with previous ion scattering results, we have found evidence for some degree of intermixing that decreases with film thickness. Such intermixing at low temperature of deposition is probably driven by place exchange between the incoming Fe and Ag atoms. An interplay between interlayer mass transport, promoting the quasi-2D growth, with exchange processes is probable, in particular at the very initial stages of growth; in this respect, the data seem to reflect an ''intermixed'' Stranski-Krastanov mode, according to the terminology introduced in Ref. 44.

This work provides solid bases for future studies on Fe/Ag and related systems. It shows that even at low temperatures it is not possible to obtain structural long-range order accompanied by film compositional purity. From another point of view, it suggests that ultrathin iron films on Ag(100) deposited at low temperature can represent an interesting system to study the influence of order and composition on surface magnetism.

ACKNOWLEDGMENTS

The authors are most grateful to Professor Giovanni Boato and Professor Andrea C. Levi for fruitful discussions and thank Antonio Gussoni and Emilio Cavanna for helpful technical assistance.

APPENDIX

We have taken into account that the substrate, as ''seen'' by the diffractometer, consists of two terraces, hereafter indicated by the subscripts u and d separated by a monatomic step. At 2, 3, 4, and 5 ML coverage a three-level system is deposited over each terrace. For simplicity we refer to the three active levels as 1, 2, and 3 (rather than $\overline{J}-1$, $\overline{J}$, and $\overline{J}+1$ as in the text). $\theta_{1u(d)}$, $\theta_{2u(d)}$, and $\theta_{3u(d)}$ are the coverages of the levels on the upper (lower) terrace. We can write

$$\theta_{1u}+\theta_{2u}+\theta_{3u}=\frac{A_u}{A}, \tag{A1}$$

$$\theta_{1d}+\theta_{2d}+\theta_{3d}=\frac{A_d}{A}, \tag{A2}$$

where A_u and A_d are the areas of terrace u and d, respectively, and $A=A_u+A_d$ is the area seen by the diffractometer.

It is reasonable, under the present experimental conditions (substrate terraces are large, a few hundred angstroms) that the *same* three-level system has grown on each terrace, so that the ratio θ_{iu}/θ_{id} does not depend on the level $i=1,2,3$ and is equal to the ratio $x=A_u/A_d$. Then, for each level i we may write

$$\theta_{iu}=x\,\theta_{id} \tag{A3}$$

and we can express the coefficients c_l of Eq. (2.2) as

$$c_0=(1+x^2)(\theta_{1d}^2+\theta_{2d}^2+\theta_{3d}^2), \tag{A4}$$

$$c_1=x(\theta_{1d}^2+\theta_{2d}^2+\theta_{3d}^2), \tag{A5}$$

$$c_1'=(1+x^2)(\theta_{1d}\theta_{2d}+\theta_{2d}\theta_{3d}), \tag{A6}$$

$$c_2'=(1+x^2)(\theta_{1d}\theta_{3d}), \tag{A7}$$

with

$$\theta_{1d}+\theta_{2d}+\theta_{3d}=\frac{1}{1+x}. \tag{A8}$$

The rocking curves coefficients read

$$\frac{2c_1}{c_0}=\frac{2x}{1+x^2}, \tag{A9}$$

$$\frac{2c_1'}{c_0}=2\frac{\theta_{1d}\theta_{2d}+\theta_{2d}\theta_{3d}}{\theta_{1d}^2+\theta_{2d}^2+\theta_{3d}^2}, \tag{A10}$$

$$\frac{2c_2'}{c_0}=2\frac{\theta_{1d}\theta_{3d}}{\theta_{1d}^2+\theta_{2d}^2+\theta_{3d}^2}. \tag{A11}$$

We could deduce x and the coverages θ_{id} from Eqs. (A8)–(A11) and then find $\theta_{iu}=x\theta_{id}$. Indeed, we are interested only in the ''total'' coverage of the ith level defined as

$$\theta_i=\theta_{iu}+\theta_{id}. \tag{A12}$$

Therefore, thanks to the proportionality expressed in Eq. (A3) we write

$$\theta_i=\theta_{id}(1+x)\quad(i=1,2,3) \tag{A13}$$

and we directly look for the θ_i's that solve the set of equations (5.3)–(5.5) as reported in the text.

---

[1] *Ultrathin Magnetic Structures I*, edited by J. A. C. Bland and B. Einrich (Springer-Verlag, Berlin, 1994).

[2] B. T. Jonker, K.-H. Walker, E. Kisker, G. A. Prinz, and C. Carbone, Phys. Rev. Lett. **57**, 142 (1986); F. Ciccacci and S. De Rossi, Phys. Rev. B **51**, 11 538 (1995).

[3] M. T. Kief and W. F. Egelhoff, Jr., Phys. Rev. B **47**, 10 785 (1993).

[4] M. Canepa, E. Magnano, Andrea Campora, P. Cantini, M. Salvietti, and L. Mattera, Surf. Sci. **352-354**, 36 (1996).

[5] M. Canepa, M. Salvietti, Andrea Campora, and L. Mattera, J. Electron Spectrosc. Relat. Phenom. **76**, 471 (1995).

[6] M. Salvietti, R. Moroni, P. Ferro, M. Canepa, and L. Mattera, Phys. Rev. B **54**, 14 758 (1996).

[7] D. A. Steigerwald, I. Jacob, and W. F. Egelhoff, Jr., Surf. Sci. **202**, 472 (1988).

[8] B. J. Hinch, C. Koziol, J. P. Toennies, and G. Zhang, Europhys. Lett. **10**, 341 (1989); C. De Beauvais, D. Rouxel, B. Bigeard, and B. Mutaftschiev, Phys. Rev. B **44**, 4024 (1991); M. Arnott, E. M. McCash, and W. Allison, Surf. Sci. **269/270**, 724 (1992); J. Duan, G. G. Bishop, E. S. Gillman, G. Chern, S. A. Safron, and J. G. Skofronick, *ibid.* **272**, 220 (1992); H. Zeng and G. Vidali, Phys. Rev. Lett. **74**, 582 (1995).

[9] H. Li, Y. S. Li, J. Quinn, D. Tian, J. Sokolov, F. Jona, and P. M. Marcus, Phys. Rev. B **42**, 9195 (1990).

[10] Hong Li and B. P. Tonner, Phys. Rev. B **40**, 10 241 (1989).

[11] J. W. Evans, Phys. Rev. B **43**, 3897 (1991).

[12] M. Henzler, Surf. Sci. **298**, 369 (1993).

[13] L. J. Gomez, S. Bourgeal, J. Ibanez, and M. Salmeron, Phys. Rev. B **31**, 2551 (1985).

[14] J. J. Harris, B. A. Joyce, and P. J. Dobson, Surf. Sci. **139**, 121 (1984).

[15] J. Lapujoulade, Surf. Sci. **108**, 526 (1981); A. C. Levi, *ibid.* **137** 305 1984; G. Armand and B. Salanon, *ibid.* **217**, 317 (1989).

[16] C. S. Lent and P. I. Cohen, Surf. Sci. **139**, 121 (1984); P. R. Pukite, C. S. Lent, and P. I. Cohen, *ibid.* **161**, 39 (1985).

[17] L. K. Verheij, B. Poelsema, and G. Comsa, Surf. Sci. **162**, 858 (1985).

[18] P. Dastoor, M. Arnott, E. M. McCash, and W. Allison, Surf. Sci. **272**, 154 (1992).

[19] J. W. Evans, D. E. Sanders, P. A. Thiel, and A. E. De Pristo, Phys. Rev. B **41**, 5410 (1990).

[20] V. Bortolani and A. Levi, Riv. Nuovo Cimento **9**, 1 (1986).

[21] George Comsa, Surf. Sci. **81**, 57 (1979).

[22] J. Falta, M. Horn, and M. Henzler, Appl. Surf. Sci. **41/42**, 230 (1989); J. Wollschläger, J. Falta, and M. Henzler, Appl. Phys. A **50**, 57 (1990).

[23] Y.-F. Liew, Y.-L. He, A. Chan, and G.-C. Wang, Surf. Sci. Lett. **273**, 1461 (1992); Q. Jiang, Y.-L. He, G.-C. Wang, Surf. Sci. **295**, 197 (1993).

[24] M. Canepa, C. Guarnaschelli, L. Mattera, M. Polese, S. Terreni, and D. Truffelli, Rev. Sci. Instrum. **62**, 1431 (1991); G. Bracco, M. Canepa, P. Cantini, F. Fossa, L. Mattera, S. Terreni, and D. Truffelli, Surf. Sci. **269/270**, 61 (1992).

[25] B. Poelsema, A. F. Becker, G. Rosenfeld, R. Kunkel, N. Nagel, L. Verheij, and G. Comsa, Surf. Sci. **272**, 269 (1992).

[26] F. James and M. Roos, MINUIT, CERN Program Library D506 (1988).

[27] H. J. Ernst, F. Fabre, and J. Lapujoulade, Phys. Rev. B **46**, 1929 (1992); D. Cvetko, V. De Renzi, L. Floreano, A. Morgante, M. Peloi, F. Tommasini, V. Chab, and K. C. Prince, *ibid.* **51**, 17 957 (1995).

[28] M. Canepa, P. Cantini, S. Terreni, and L. Mattera, Surf. Rev. Lett. (to be published).

[29] G. Comsa and B. Poelsema, in *Atomic and Molecular Beam Methods*, edited by G. Scoles (Oxford University Press, New York, 1992), Vol. 2, p. 463.

[30] R. Q. Hwang, J. Schröder, C. Günther, and R. J. Behm, Phys. Rev. Lett. **67**, 3279 (1991); T. Michely, M. Hohage, M. Bott, and G. Comsa, *ibid.* **70**, 3943 (1993); H. Brune, C. Romainczyk, H. Röder, and K. Kern, Nature (London) **369**, 469 (1994).

[31] A. Brodde, G. Wilhemi, D. Badt, H. Wengelnik, and H. Neddermeyer, J. Vac. Sci. Technol. B **9**, 920 (1991).

[32] M. H. Langelaar and D. O. Boerma, in *Thin Films—Structure and Morphology*, edited by R. C. Cammarata, E. H. Chason, D. Ila, and S. Moss, MRS Symposia Proceedings No. 441 (Materials Research Society, Pittsburgh, 1997).

[33] R. Kunkel, B. Poelsema, L. K. Verheij, and G. Comsa, Phys. Rev. Lett. **65**, 733 (1990).

[34] M. C. Bartelt and J. W. Evans, Surf. Sci. **314**, L829 (1994); A. E. DePristo and Y. Li, *ibid.* **351**, 189 (1996); K. W. Jacobsen, J. Jacobsen, and J. K. Nørskov, *ibid.* **359**, 37 (1996).

[35] M. Villarba and H. Jonsson, Surf. Sci. **317**, 15 (1994).

[36] H.-J. Ernst, F. Fabre, and J. Lapujoulade, Surf. Sci. **275**, L682 (1992).

[37] P. Bedrossian, B. Poelsema, G. Rosenfeld, L. C. Jorritsma, N. N. Lipkin, and G. Comsa, Surf. Sci. **334**, 1 (1995).

[38] W. F. Egelhoff, Jr. and I. Jacob, Phys. Rev. Lett. **62**, 921 (1989).

[39] B. T. Jonker and G. A. Prinz, Surf. Sci. **172**, L568 (1986).

[40] S. Terreni, P. Cantini, M. Canepa, and L. Mattera (unpublished).

[41] G. L. Kellogg and P. J. Feibelman, Phys. Rev. Lett. **64**, 3143 (1990); P. J. Feibelman *ibid.* **65**, 729 (1990).

[42] C. Chen and Tien T. Tsong, Phys. Rev. Lett. **64**, 3147 (1990); S. C. Wang and G. Ehrlich, *ibid.* **67**, 2509 (1991).

[43] G. L. Kellog, Phys. Rev. Lett. **67**, 216 (1991).

[44] S. Rousset, S. Chiang, D. E. Fowler, and D. D. Chambliss, Phys. Rev. Lett. **69**, 3200 (1992).

[45] Y.-L. He and G.-C. Wang, Phys. Rev. Lett. **71**, 3834 (1993).

[46] W. F. Egelhoff, Jr., in *Ultrathin Magnetic Structures I* (Ref. 1), Chap. 5, p. 220.

[47] Th. Detzel and N. Memmel, Phys. Rev. B **49**, 5599 (1994).